OPEN ACCESS
IOP Publishing
Journal of Physics D: Applied Physics
J. Phys. D: Appl. Phys. **58** (2025) 025112 (9pp)
https://doi.org/10.1088/1361-6463/ad8662

Impact of stacking faults on the luminescence of a zincblende InGaN/GaN single quantum well

Abhiram Gundimeda[1], Gunnar Kusch[1,*], Martin Frentrup[1], Huixin Xiu[1,2], Ruiying Shu[3], Christina Hofer[3], Paul A J Bagot[3], Michael P Moody[3], Menno J Kappers[1], David J Wallis[1,4] and Rachel A Oliver[1]

[1] Department of Materials Science and Metallurgy, University of Cambridge, 27 Charles Babbage Rd, Cambridge CB3 0FS, United Kingdom
[2] School of Materials and Chemistry, University of Shanghai for Science and Technology, 516 Jungong Road, Yangpu District, Shanghai 200093, People's Republic of China
[3] Department of Materials, University of Oxford, Parks Road, Oxford OX1 3PH, United Kingdom
[4] Centre for High Frequency Engineering, University of Cardiff, 5 The Parade, Newport Road, Cardiff CF24 3AA, United Kingdom

E-mail: gk419@cam.ac.uk

Received 23 July 2024, revised 20 September 2024
Accepted for publication 14 October 2024
Published 24 October 2024

Abstract

In this paper, we investigate the optical properties of a zincblende InGaN single quantum well (SQW) structure containing stacking faults (SFs). Cathodoluminescence studies revealed the presence of sharp emission features adjacent to SFs, identified as quantum wires (Qwire) via their spatial anisotropy. Scanning transmission electron microscopy provided evidence of indium rich regions adjacent to SFs which intersect the QW along the [110] and [1–10] directions, whilst atom probe tomography revealed that the indium rich regions have an elongated structure, creating a Qwire. This work sheds light on the intricate relationship between SFs and Qwires in zincblende InGaN SQW structures, offering insights into the underlying mechanisms governing their optical behavior.

Supplementary material for this article is available online

Keywords: zincblende, cathodoluminescence, quantum well, stacking faults, quantum wire

1. Introduction

Micro light-emitting diode (microLED) technology has emerged as a transformative force in display applications such as wearable devices for augmented reality, offering unprecedented advantages in terms of energy efficiency, brightness, and pixel density and also holds promise for high-speed visible light communications [1]. InGaN-based light-emitting diodes (LEDs) based on quantum well (QW) structures have already revolutionized solid-state lighting due to their superior material qualities [2, 3], and are poised to make an equally pivotal contribution to the microLED field. The prevailing commercial standard for InGaN-based devices involves polar wurtzite (wz) structures grown in the [0001] *c*-direction. While device structures have proven successful, the polar crystal orientation introduces internal electric fields that, in QW structures, give rise to the quantum confined Stark effect (QCSE), separating

* Author to whom any correspondence should be addressed.

electrons and holes. This in turn leads to an increased carrier lifetime, an emission energy dependence on the carrier density in the QW and a strong reduction in the internal quantum efficiency. In the case of blue LEDs, these issues can be mitigated by reducing the QW thickness, thereby minimizing the separation of electrons and holes and achieving impressive quantum efficiencies of up to 85% [2]. However, challenges persist for longer wavelength nitride LEDs. For example, green LEDs grown in the *c*-direction, struggle to surpass quantum efficiencies beyond 35%, thus lagging behind their blue counterparts in development [2]. Green LEDs face additional hurdles, primarily associated with the higher amount of InN required for green-emitting QWs, leading to increased emission energy non-uniformity, diminished spectral purity of devices, and heightened droop due to locally higher carrier densities [4–7].

In the pursuit of enhanced efficiency in green and longer wavelength LEDs, various avenues have been explored. One promising approach involves the growth of semi- or non-polar crystal orientations of wz-GaN-based material. This approach offers the benefits of growing in the thermodynamically stable wz crystal structure of III-nitrides while simultaneously reducing or strongly limiting the adverse effects of the QCSE. Despite considerable research efforts invested in this path, green LEDs based on non- and semi-polar crystal orientations have yet to match the efficiencies achieved by polar *c*-plane LEDs. This discrepancy can be attributed to an array of intrinsic issues, including the necessary use of QWs with higher InN contents (due to the absence of the QCSE-related redshift) but exacerbated by a reduced indium incorporation of (some) non- and semi-polar planes and an increased incorporation of impurities and intrinsic point defects [2, 6, 8]. Furthermore, a high density of (non-radiative) basal plane stacking faults (SFs) tend to form at the GaN/hetero-substrate interface requiring the use of lateral-overgrowth techniques or the use of bulk GaN substrates.

Although the commercial standard predominantly still favors *c*-plane InGaN QWs for green light emission, recent investigations have highlighted the unique advantages offered by zinc-blende (zb) InGaN, ushering in a renewed interest in this crystal structure. Zb-InGaN can be free of piezoelectric fields when grown in the (001) orientation, due to its cubic symmetry [6, 9]. This can theoretically avoid any polarization-induced electric fields within the QW, removing the QCSE. The absence of the piezoelectric fields means that the electron–hole wavefunction overlap should be strongly enhanced when compared to conventional hexagonal *c*-plane devices, reducing carrier lifetimes and dependence of the emission wavelength on the operating conditions, as well as improving the internal quantum efficiency. Zb-InGaN QWs additionally have a lower bandgap than their wz counterparts (i.e. 3.3 eV in comparison to 3.5 eV for GaN [10]), reducing the amount of indium needed to reach long wavelength emission.

While the potential advantages of zb-InGaN QWs are apparent, there are plenty of challenges which need to be resolved. It is thus not yet possible to fabricate zb-InGaN LEDs whose performance is competitive with their wz counterparts. Due to the lack of inexpensive native substrates, zb-GaN is often grown on a 3C-SiC/Si substrates, primarily chosen for its small lattice mismatch (3.4% between 3C-SiC and zb-GaN) and the cubic structure of the 3C-SiC polytype, which acts as a template for the zb-GaN growth [11, 12]. However, the growth of zb-GaN on lattice mismatched 3C-SiC/Si substrates leads to the formation of SFs, i.e. monolayers of wz-GaN in the zb-GaN lattice. Such SF formations are attributed to the dissociation of perfect dislocations into energetically preferred partial dislocations at the heterointerface [13] and the preferred incorporation of wz-GaN owing to it being the thermodynamically more stable phase [14, 15]. These structural defects possess the capacity to impact the electronic and optical characteristics of the material [16, 17]. Given their potential deleterious effects on light output efficiencies, a thorough investigation into the effect of SFs on the optical properties of zb-InGaN/GaN QW structures is worthwhile.

To investigate the influence of SFs on the optical properties, we utilized cathodoluminescence (CL) spectroscopy which can spatially resolve and characterize the emission properties of zb-InGaN/GaN structures at the nanoscale. This enables us to correlate structural defects with variations in the emission spectra, elucidating their impact on the material's optoelectronic performance. In previous work [18], we have shown that the emission from a zb-GaN single QW (SQW) structure exhibits a strong inhomogeneity both in the emission energy and the emission peak intensity, but that the local full width at half maximum (FWHM) from limited areas was comparable to that of *c*-plane QWs [19]. We attributed the observed spectral variations to QW thickness fluctuations, variations in the InGaN alloy composition near SFs as well as, very occasionally, emission from semipolar SQWs formed locally at wz inclusions [20]. Furthermore, it was shown that individual SFs and SF bunches in zb-QW structures are associated with local non-radiative recombination centers, leading to a reduced light emission intensity [18]. Such regions with high density of SFs were suggested to suffer from stronger efficiency droop under high excitation conditions, in comparison to SF-free regions. On a microscopic scale, indium segregation was discovered next to SFs using scanning TEM (STEM) energy dispersive x-ray spectroscopy (EDS) studies [16, 20]. Scanning electron microscopy (SEM)-CL studies on the same site-specific TEM cross section lamella demonstrated that in addition to the QW emission, several low energy peaks were also evident in the CL spectra. These low-energy peaks were found to be associated with SF bunches intersecting the QWs [20]. These observations suggest that the poor spectral purity of the macroscopic emission spectrum from such zb-QWs can be attributed in part to the local impact of SFs on indium incorporation.

In the present CL study, we focus our investigation on the optical characteristics associated with SFs in zb-InGaN QWs. We specifically explore the nature of emission from SF-related structures in a zb-SQW sample, addressing the formation of quantum structures of reduced dimensionality.

2. Experimental details

The sample investigated here is the same SQW structure as previously studied by power dependent CL [18]. It consists of an ≈800 nm-thick zb-GaN epilayer grown by metal organic vapor phase epitaxy under standard growth conditions on a (001) oriented 3C-SiC/Si pseudo-substrate with 4° miscut. This was followed by a 40 nm-thick $In_xGa_{1-x}N$ underlayer ($x \approx 0.01$–0.02), a nominally 2 nm-wide $In_{0.1}Ga_{0.9}N$ SQW and capped by an 8 nm-thick GaN layer. Further details of the structure and the growth details can be found elsewhere [18]. In previous studies of similar materials, we assumed that that the miscut direction was along [110]. However, in this work we follow the findings of our recent detailed electron microscopy study, which has shown that based on the atomic arrangements the miscut points towards the crystallographic [1–10] zb-GaN direction [21].

An Allalin 4027 Chronos SEM CL system with a 150 l mm^{-1} grating (blazed at 500 nm) was employed for low temperature hyperspectral CL measurements and secondary electron (SE) imaging at 10 K. For the optical characterization of the SQW sample an excitation voltage of 3 kV and a beam current of 63 pA were used. A Monte Carlo simulation, using the software Casino [22], shows that the interaction volume reaches to about 47 nm from the sample surface where incident electrons lose 90% of their energy, which covers the SQW. Under these conditions, our previous studies [18] have shown high emission intensities and no beam damage to the sample.

A FEI Tecnai Osiris microscope, equipped with a high-brightness XFEG source and four-EDS-detector SuperX system, was utilized for high-angle annular dark-field (HAADF) STEM imaging, TEM imaging and EDS measurements on the SQW sample. The microscope was operated at 200 kV with a beam current of 80 pA. Cross-sectional, electron-transparent, thin foils were prepared using a FEI Helios NanoLabTM focused ion beam microscope with *in-situ* lift-out. A 1 μm-thick Pt metal layer was deposited, to protect the surface, followed by Ga ion milling at 30 kV and a final 5 kV treatment to reduce ion damage to make a lamella of about 80 nm to 120 nm thickness.

For atom probe tomography (APT) analysis the samples were coated with a 20 nm thick chromium layer using a Leica EM ACE600 high vacuum sputter coater to protect the surface. Subsequently, the APT specimens were prepared using a Zeiss XBeam SEM/focused ion beam (FIB) instrument following the standard lift-out procedure described in [23]. The final FIB polishing step was performed at 2 kV to minimize beam damage [24]. APT experiments were carried out using a local electrode atom probe (CAMECA LEAP 5000 XS) with 500 kHz pulsed UV laser excitation (355 nm), while maintaining the specimen temperature at 50 K in ultra-high vacuum. A laser pulse energy of 10 pJ was applied. For visualization and analysis, the IVAS 6.3 software was employed. The 3D reconstruction was initially generated based upon the profile of the applied-voltage, and subsequently calibrated using the known thicknesses of the SQW and $In_xGa_{1-x}N$ underlayer, respectively.

3. Results and discussion

3.1. Low dimensional quantum emissions

The representative SE image of the zb-InGaN/GaN SQW structure in figure 1(a) shows a rich microstructure with flat regions and elongated surface features aligned along both in-plane ⟨110⟩ directions. Pale stripes aligned in the same directions have been previously associated with planar {111} SFs terminating at the (001) sample surface [18]. The region shown in figure 1 is ideal to study the influence of SFs on the optical transitions in the SQW sample, as it exposes regions with high densities of SFs as well as SF-free regions. In the panchromatic CL map in figure 1(b), regions with high SF density appear dimmer compared to the bright regions free from SFs. From the measured hyperspectral map, we have extracted representative spot spectra in regions that are apparently SF-free and SF-rich.

As highlighted in the SE image (figure 1(a)), the spot S1 corresponds to an undisturbed region, apparently free from SFs, for which the corresponding panchromatic image shows high intensity QW emission. Here, the normalized spectrum displayed in figure 1(d) exemplifies the characteristic behavior of the QW, aligning with the overall mean spectrum of the sample as reported previously [18]. The spot spectrum taken at S1 shows a QW emission peak centered at around 2.95 eV to 3.00 eV with a FWHM of about 175 meV. Additionally, a broad, low-energy tail is observed, which can be attributed to compositional and thickness inhomogeneities in the QW. In contrast, the emission intensity from the SF-rich region (spot S2), as visualized in the panchromatic CL image (figure 1(b)), is approximately two orders of magnitude weaker. The emission energy at S2 is slightly red-shifted which may be associated with enhanced In incorporation at SFs. The corresponding spot spectrum reveals a significantly broader emission peak with a FWHM of 247 meV. The substantial reduction in intensity may be related to non-radiative recombination centers located at SFs [18]. The spot spectrum S3 was obtained from a region on the edge of a SF (or SF bunch) that runs parallel to the [1–10] miscut direction. Similar to spot S2, the intensity of the emission is significantly reduced at S2. In addition to the QW emission peak, multiple sharp emission peaks can be observed at lower energies. In the specific case shown here, these peaks have energies of 2.43 eV, 2.50 eV, and 2.53 eV and have a FWHM of about 20 meV for each of these peaks. The spectral resolution of the instrument, at the conditions used for this measurement, is about 4 meV. However, while spot spectra taken in many SF-rich regions include sharp, low energy peaks, their specific emission energy strongly varies between different regions. The location of these spectral features on or close to SF bundles indicate a strong role of the SFs in their formation mechanism.

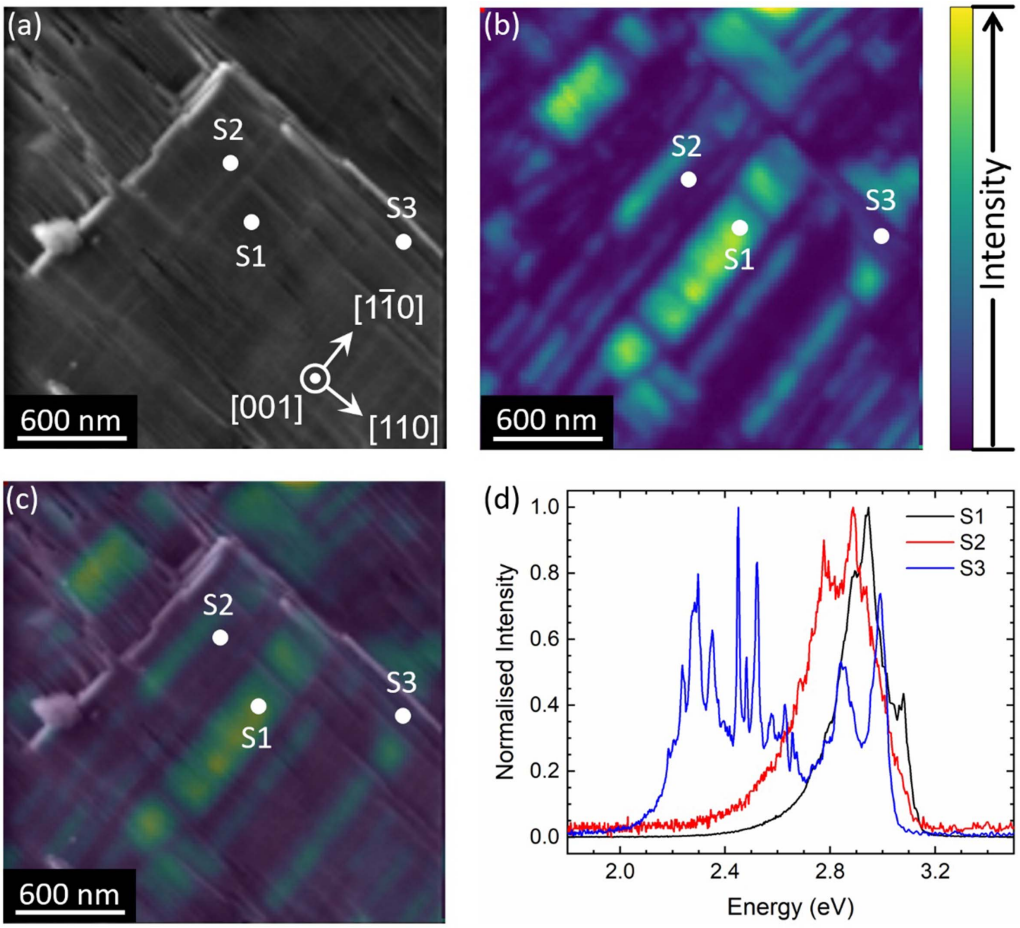

Figure 1. (a) SE image of the zb-InGaN/GaN SQW structure and (b) the simultaneously recorded panchromatic CL image. (c) An overlay of the SE image and the panchromatic CL intensity image, indicating the positions S1, S2 and S3 from where spot spectra have been taken. (d) Normalized spot spectra from spot S1, S2 and S3. All data were recorded at a temperature of 10 K.

Such narrow optical emission is likely caused by enhanced carrier confinement in the specific region, which can be attributed to either quantum wire (Qwire) or quantum dot (QD) like structures.

In a first step to explore the exact nature of these low energy, sharp emission peaks measured near SFs, we determined the in-plane extent of these features. For this purpose, we have first identified various SFs (or SF bunches) based on the location of pale stripes in the SE image. In a second step, line spectra along and across the SFs have been extracted from the related region of the hyperspectral CL map for further examination. An example for such an analysis is presented in figure 2, where the region in the bottom right of the SE image (figure 2(a)) shows SF features marked as SF1, SF2, SF3, and SF4. (To help with visualization of the features relating to SF1–SF4, we also include in the supplementary material figures S1 and S2, which for each of figures 2(a) and (b) respectively provide a version of the image with less labels, and a zoomed in image of the main region of interest, with the contrast enhanced.) Line spectra were then extracted parallel (I) and perpendicular (II) to the SF-line direction as indicated by the red dashed arrows in the SE image (figure 2(a)) and the corresponding panchromatic CL image (2 (b)).

Figure 2(c) shows the line scan map extracted along SF2, in the [1–10] direction (I), while in figure 2(d) the CL spot spectrum taken at the point marked by a yellow dashed line in (c) highlights several emission features. The line scan shows QW emission at ca. 3.00 eV along the whole length of the scan. Along with the QW emission, sharp emission peaks were also observed with emission energies of 2.63 eV, 2.56 eV, and 2.47 eV respectively. The spatial extent of the features along the SF was obtained from the length in the line maps for which emission intensity was observed at their specific energy. At an emission energy of 2.63 eV, two individual features were observed whose lengths were measured to be 175 nm and 75 nm. It might be that these belong to a single long feature interrupted by a region with strong non-radiative recombination running across it. However, a more detailed analysis to identify this feature was limited by the rich surface morphology. Similarly, the length of the two features emitting at 2.56 eV in the line scan was determined to be 30 nm and 60 nm. A statistical analysis over 16 different

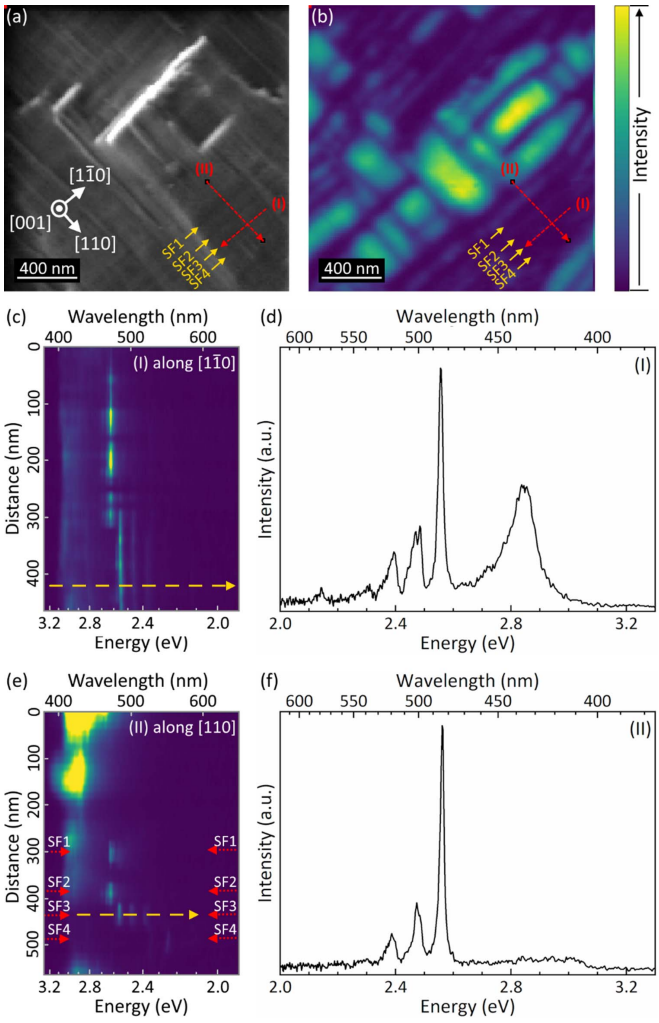

Figure 2. (a) SE image of a zb-InGaN/GaN SQW structure and (b) simultaneously recorded panchromatic CL image. (c) Line scan taken parallel to the miscut direction, along [1–10] that covers a region of several parallel SFs. (d) CL spectrum taken at a certain point (marked by a yellow dashed line in (c)) highlighting several quantum emissions. (e) Line scan taken perpendicular to the miscut direction, along [110] that covers the region of several SFs (SF1-4). (f) CL spectrum taken at SF3 (marked by a yellow dashed line in (e)) showing various quantum emissions.

regions across four separate data sets revealed that the average length along the SF (in the [1–10] miscut direction) for which sharp emission was observed is (130 ± 10) nm. This length is significantly larger than the electron wavefunction in GaN, which suggest that little to no carrier confinement is occurring in this direction. Consequently, the origin of the sharp peaks along the SFs is unlikely to be related to QD like features.

To measure the extent of these features along the perpendicular [110] direction, the line scan in figure 2(e) was extracted from the hyperspectral map perpendicular to the SFs. The position of the SFs observed in the SE image are marked on the line map. The map reveals that at each SF at least one sharp emission feature can be observed. For the SFs labeled as SF1 and SF2, the emission energy of the feature is at 2.63 eV. For SF3, three such sharp emissions can be observed with emission energy peaks at 2.56 eV, 2.47 eV, and 2.39 eV. These are also visible in the spot spectrum from SF3 in figure 2(f). The emission peak at SF4 was centred at 2.25 eV. A statistical analysis over eight different regions in four SE images revealed that the average width of the sharp emission features perpendicular to the SF line direction is only (45 ± 15) nm. This indicates that these sharp features have an asymmetric shape, thus elongated in one direction only, which suggests the formation of Qwire-like structures. The direction of elongation is parallel to the SFs.

It is important to state here, that the width of the features as measured by the CL line spectrum is likely limited by the size of the interaction volume (diameter of 47 nm for 90% of incident electron energy loss) and presents an upper limit of the feature size, as dimensions smaller than the interaction volume cannot be resolved accurately. Another possibility for the nature of an asymmetric feature might be the formation of a line of QDs. In this case, different QDs would be expected to exhibit different emission wavelengths due to small variations in dot size as well as dot composition. However, this is not supported by our observations as some features in our sample are several tens of nanometre long with a single emission wavelength for that feature, which rules out the clustering of QDs and makes Qwire-like features a more likely explanation.

3.2. *InGaN Qwire formation*

To gain a better understanding of the origins of Qwire-like emission at SFs, STEM imaging was performed of SFs intersecting the QW. Figure 3(a) shows a cross-sectional HAADF STEM image of a typical area featuring the SQW and several SFs. The QW is visible by its bright contrast with ill-defined top and bottom boundaries, indicating that the QW was grown on a wavey surface. In the middle of the image, next to the SQW several diagonal dark lines, parallel to each other, are visible. These lines are caused by a bunch of {111}-type SFs in the InGaN underlayer that intersect the QW. The appearance of an about 2 nm-wide, high-contrast stripe parallel to and to the left of the SF bunch suggests the accumulation of heavier elements, likely indium, next to the SF within the InGaN underlayer and the QW. This phenomenon is observed for most of the SFs that run to the surface intersecting the QW. The enrichment of indium was confirmed by a STEM EDS analysis. Figure 3(b) shows the elemental map of indium for the area shown in the HAADF image. Correlating the HAADF image with the elemental map reveals an increased indium incorporation and a slight depletion of gallium along the bright stripe in the HAADF image. Interestingly this indium segregation seems to occur only on one side of the SF bunch but not on the other, as highlighted by the schematic drawing in figure 3(c). The STEM measurements show that the spatial dimension of this compositional increase is on the order of 2 nm, well within the range to provide carrier confinement.

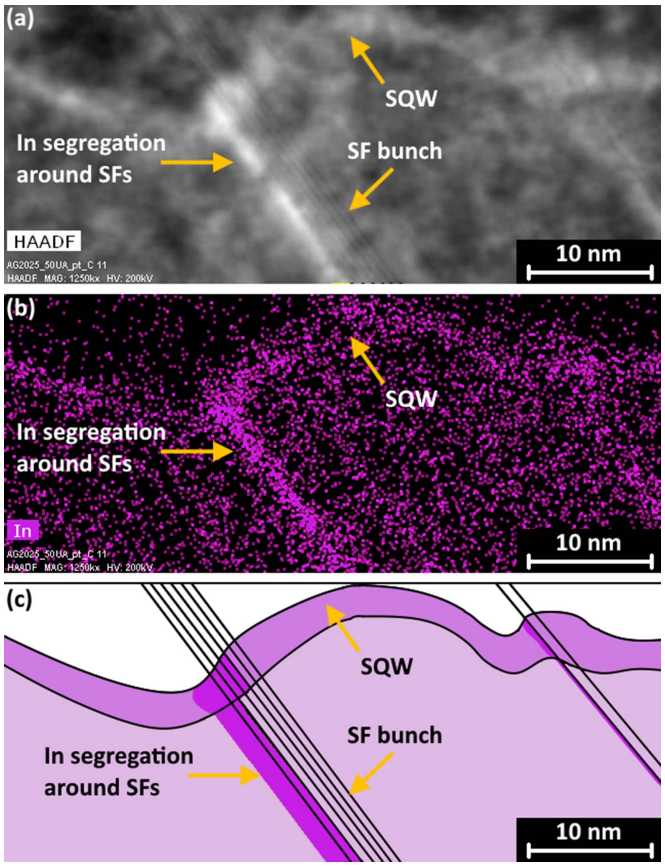

Figure 3. (a) A cross-sectional HAADF image of the zb-InGaN underlayer and zb-InGaN SQW along with (b) the STEM-EDS elemental map of in (purple). (c) Schematic drawing highlighting the position of the SQW and the in segregation around a bunch of SFs.

To support the STEM studies, we have also used APT to image the QW structure. Whilst in our STEM datasets we see a 2D projection of the 3D structure, APT is able to provide 3D compositional information. Figure 4(a) shows a reconstruction of the APT sample containing a SQW near the apex of the sample and the InGaN underlayer beneath it. Here Ga atoms are rendered in yellow and In atoms in purple. In figure 4(b) we show a close-up of the region of the sample near the apex, where the indium-containing layers are found. This render, in which the InGaN layers are viewed in cross-section, is strikingly similar to figure 3, in that we see an indium rich region, cutting diagonally thorough the InGaN underlayer and intersecting the QW. This is observable in both the original atom map and when an In site fraction iso-concentration surface ('iso-surface') is superimposed at 3.2% In. (The indium site fraction is the fraction of the group III atoms which are In). Based on comparison with the STEM-EDX data, we attribute this inclined feature to In segregation adjacent to a SF.

Viewing the QW in plan view (figure 4(c)), we see the intersection of the inclined feature and the QW as an elongated region of enhanced indium content. This is visible in an In site fraction iso-surface at 4.6% In, and in a 2D heat map of the In site fraction. Two further such elongated regions can be seen in the plan view iso-surface running roughly perpendicular to the first feature, although these features are less obvious in the heat map. Considering the most pronounced feature, its width appears to be roughly 10 nm, and its length exceeds the field-of-view of the APT data set, and is thus greater than 45 nm. Hence, although we are not able to directly correlate the size of the feature to the sizes of the Qwires observed in SEM/CL due to the limited extent of the APT data set, these data provide strong evidence for the existence of elongated In-rich regions. Further APT data on these materials, and more in-depth discussion of APT on zb nitrides will be the subject of a future manuscript.

Together, the APT and STEM data show that when the planar InN-enriched regions in the InGaN underlayer parallel to the {111} SFs intersect with the QW, they lead to elongated, highly InN-enriched stripes along the ⟨110⟩ intersection line, in which carriers can be confined in two directions. This is in good agreement with results from Ding *et al* [16] and Church *et al* [17], who also observed InN agglomeration close to SFs in cross-sectional STEM images. They observed that near the SFs intersecting zb-InGaN QWs the InN concentration is substantially increased, compared to the undisturbed QW. It is therefore reasonable to assume that the narrow, InN-enriched, elongated features in the QW next to SFs are the origin for the sharp Qwire-like emission peaks at energies below the QW emission energy. This agrees well with the work by Church *et al* [17], who suggest that the Qwire-like features result in a broad, low energy peak in their photoluminescence measurements: we similarly observe the sharp Qwire-like features across a broad range of energies, to the low energy side of the main QW peak. We note that although, consistent with the earlier work of Ding *et al* [16],we here initially suggest that the formation of Qwire-like structures is related to compositional segregation, in this particular case the existence of both the segregation adjacent to the plane of the inclined SF and the intentionally-indium rich SQW creates two intersecting planes of In-rich material—effectively two QWs. Someya *et al* [25] have previously shown that two intersecting GaAs QWs in a somewhat similar morphology, can create a Qwire with a T-shaped cross section, and it is possible that the distorted T-shaped intersection here may have a similar impact.

In the discussion above, it is important to emphasize that the indium segregation is next to one side of the SF, confirming previous results [16]. Since SFs could be seen as wz inclusions in a zb matrix, carriers generated within the SF are expected to lower their energy by diffusing to adjacent regions, where they could recombine radiatively. However, we have previously noted that SFs appear dark in CL [18], suggesting that point defects either within or adjacent to the SFs act as non-radiative recombination centers. If carriers from the SF could diffuse to adjacent high In-content Qwires and recombine radiatively, we would not expect the SFs to appear dark in CL. Hence, the existence of such Qwires might imply that

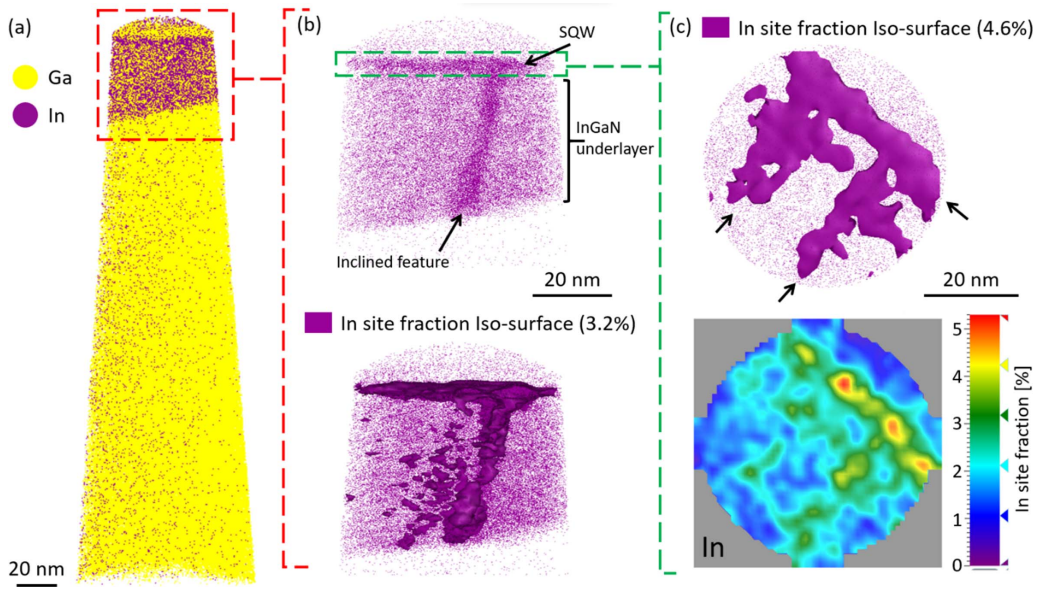

Figure 4. (a) APT reconstruction containing the InGaN QW and underlayer region highlighted by a red dashed box. Ga atoms are shown in yellow and in atoms in purple. (b) Above: A zoomed-in view of in distribution in the SQW & in underlayer region. Below: the purple iso-surfaces highlights the in segregation (c) above: the purple iso-surfaces show the In segregation within the SQW in plan view. Below: A 2D site fraction map of the distribution of in along the SQW in plan view.

carriers generated within the SF cannot diffuse to the Qwires but instead recombine non-radiatively at point defects within the SF itself. However, this point requires further investigation.

Overall, we conclude that the emergence of sharp, highly localized peaks evident in the CL maps is associated with the presence of Qwires, formed adjacent to where SFs intersect the QW. As noted above, these findings align closely with recent observation by Church *et al* [17]. As well as suggesting that their low energy peak might relate to Qwire formation, they showed that this emission is strongly polarized perpendicular to the miscut direction (here along the [110] direction), while the high energy emission band shows a much lower polarization degree. If the highly polarized low energy emission relates to the Qwire, then one might expect to find an anisotropy in the SF density [26]. We will investigate this possibility in the next section.

3.3. Statistical quantification of quantum emitters

The plan-view bright-field TEM image shown in figure 5(a) shows the surface of a zb-GaN epilayer (similar to that used for the SQW sample) bisected by SFs aligned in both ⟨110⟩ in-plane directions. The SF network is composed of rectangles with mostly short [1–10] and long [110] sides, indicating that the density of [110]-aligned SFs is higher than that of the [1–10]-aligned SFs (running perpendicular and parallel to the miscut direction respectively), in agreement with previous TEM studies [26]. A detailed analysis of the TEM image revealed a a density of [110]-aligned SFs of 1.6×10^5 cm^{-1} and a density of [1–10]-aligned SFs of 8.9×10^4 cm^{-1}. The average size of the SFs at the surface varies very strongly between a few tens of nanometers up to a few hundred nanometers.

As shown in the previous sections, Qwire-like emission adjacent to SFs is observed by SEM-CL. To observe how the Qwire features are distributed in emission energy and orientation, a quantitative analysis was performed across five SEM-CL images. For this purpose, several SFs are identified in the SE images parallel and perpendicular to the [1–10] miscut direction, followed by the identification of the position and alignment of the Qwires from the hyperspectral maps. As we have seen in the previous section that some Qwire features have widths of 30 nm, it is important to note that the selected Qwire features have a length of at least 60 nm, which corresponds to 4 pixels in a map. Overall, the histogram in figure 5(b) shows that the Qwires are predominantly [110]-aligned, that is perpendicular to the [1–10] miscut direction. In comparison, detection of Qwires aligned parallel to the miscut direction, i.e. along the [1–10] direction, are relatively rare. Interestingly, the emission energy also shows a strong dependence on the in-plane alignment of the Qwires. Those aligned along [1–10] expose an average emission energy centered at around 2.64 eV (470 nm). The average emission energy of the Qwire features aligned along [110] is centered around 2.48 eV (500 nm), which is significantly redshifted. The average lengths of the Qwire features were calculated to be around (130 ± 10) nm which is in good agreement with the plan-view TEM measurements on similar zb-GaN samples. In comparison with the work in [17] the one-dimensional nanostructures relating to the low energy PL emission that was polarized along the axis perpendicular to the sample miscut might be related to the Qwires aligned along [110] associated with

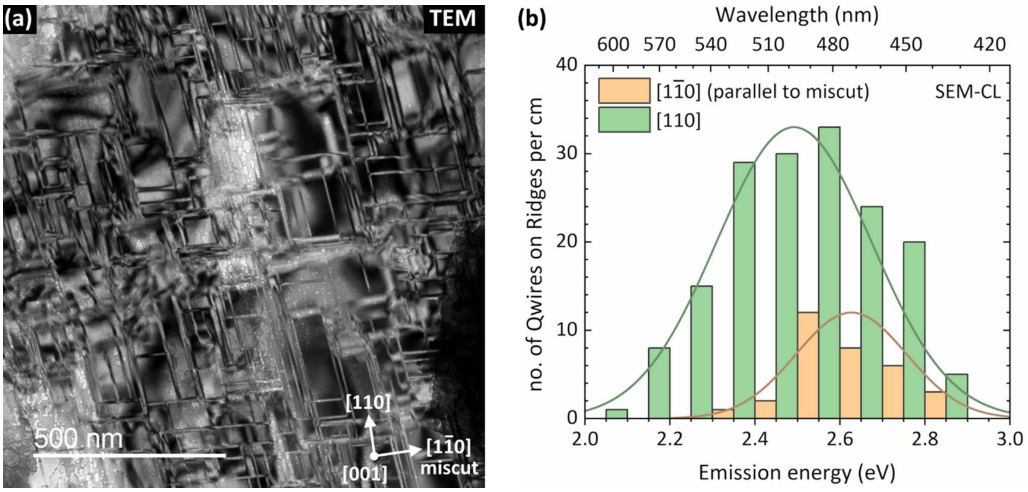

Figure 5. (a) Plan-view bright-field TEM image of a typical zb-GaN epilayer showing an anisotropic distribution of SFs. A lower density of SFs parallel to the [1–10] miscut direction than perpendicular to it can be observed. (b) Density and emission energy distribution of Qwire-like emission centers from surface features in SEM-CL that are running parallel to the miscut direction, i.e. along [1–10] (orange), and perpendicular to the miscut direction, along [110] (green).

sharp peaks emitting over a wide energy range but redshifted relative to the QW peak as discovered in this work.

4. Conclusions

CL analysis of regions containing SFs in a (001) oriented zb-InGaN SQW structure revealed the presence of highly localized, sharp emission features adjacent to the SFs. Combining STEM and APT, these features were identified as being related to QWires, which form due to the segregation of indium adjacent to the SFs. These Qwire emissions with varied emission wavelengths were observed near several SFs intersecting the QW both parallel to the sample miscut (along [1–10]) and perpendicular to it (along [110]). Additionally, a quantitative analysis of the Qwire CL emission energies showed that there was an anisotropic distribution of these Qwire features. These Qwires ran predominantly along [110], perpendicular to the miscut direction, which is consistent with the distribution of SF orientations in similar material. Given that emission from such Qwires is expected to be polarized, the anisotropy of the QWire orientation is expected to lead to an overall polarization of the QW emission, particularly in the long wavelength tail of the emission.

Data availability statement

The data that support the findings of this study are openly available at the following URL/DOI: https://doi.org/10.17863/CAM.112895.

Acknowledgment

This work was enabled through financial support by Innovate UK through the Energy Catalyst Round 2—Early Stage Feasibility scheme (Ref. 132135): ‘To demonstrate the potential to make low cost, high efficiency LEDs using 3C-SiC substrates’, and by EPSRC through platform Grant No. EP/M010589/1: ‘Beyond Blue: New Horizons in Nitrides’ and research Grant No. EP/R01146X/1: ‘Fundamental studies of zincblende nitride structures for optoelectronic applications’. D J Wallis would like to thank the support of EPSRC through Grant No. EP/N01202X/2. The CL facility was funded by EPSRC under EP/R025193/1. The APT facility was funded by EPSRC under EP/S021663/1: ‘A LEAP 5000 XS for the UK National Atom Probe Facility’.

ORCID iDs

Gunnar Kusch https://orcid.org/0000-0003-2743-1022
Rachel A Oliver https://orcid.org/0000-0003-0029-3993

References

[1] Ding K, Avrutin V, Izyumskaya N, Özgür Ü and Morkoç H 2019 Micro-LEDs, a manufacturability perspective *Appl. Sci.* **9** 1206
[2] Monavarian M, Rashidi A and Feezell D 2018 A decade of nonpolar and semipolar III-nitrides: a review of successes and challenges *Phys. Status Solidi* a **216** 1800628
[3] Zhou C, Ghods A, Saravade V G, Patel P V, Yunghans K L, Ferguson C, Feng Y, Kucukgok B, Lu N and Ferguson I T 2017 Review—the current and emerging applications of the III-nitrides *ECS J. Solid State Sci. Technol.* **6** Q149
[4] Ren C X 2016 Polarisation fields in III-nitrides: effects and control *Mater. Sci. Technol.* **32** 418
[5] Auf der Maur M, Pecchia A, Penazzi G, Rodrigues W and Di Carlo A 2016 Efficiency drop in green InGaN/GaN light

emitting diodes: the role of random alloy fluctuations *Phys. Rev. Lett.* **116** 027401
[6] Binks D J, Dawson P, Oliver R A and Wallis D J 2022 Cubic GaN and InGaN/GaN quantum wells *Appl. Phys. Rev.* **9** 041309
[7] Massabuau F C-P *et al* 2014 The impact of trench defects in InGaN/GaN light emitting diodes and implications for the "green gap" problem *Appl. Phys. Lett.* **105** 112110
[8] Kusch G, Frentrup M, Hu N, Amano H, Oliver R A and Pristovsek M 2022 Defect characterization of 10–13 GaN by electron microscopy *J. Appl. Phys.* **131** 35705
[9] Lee L Y 2017 Cubic zincblende gallium nitride for green-wavelength light-emitting diodes *Mater. Sci. Technol.* **33** 1570
[10] Vurgaftman I and Meyer J R 2003 Band parameters for nitrogen-containing semiconductors *J. Appl. Phys.* **94** 3675–96
[11] Cheung R 2006 *Silicon Carbide Microelectromechanical Systems for Harsh Environments* (Published by Imperial College Press and Distributed by World Scientific Publishing Co)
[12] Frentrup M, Lee L Y, Sahonta S-L, Kappers M J, Massabuau F, Gupta P, Oliver R A, Humphreys C J and Wallis D J 2017 x-ray diffraction analysis of cubic zincblende III-nitrides *J. Phys. D: Appl. Phys.* **50** 433002
[13] Vacek P, Frentrup M, Lee L Y, Massabuau F C-P, Kappers M J, Wallis D J, Gröger R and Oliver R A 2021 Defect structures in (001) zincblende GaN/3C-SiC nucleation layers *J. Appl. Phys.* **129** 155306
[14] Wright A F 1997 Basal-plane stacking faults and polymorphism in AlN, GaN, and InN *J. Appl. Phys.* **82** 5259–61
[15] Glas F 2008 A simple calculation of energy changes upon stacking fault formation or local crystalline phase transition in semiconductors *J. Appl. Phys.* **104** 093520
[16] Ding B, Frentrup M, Fairclough S M, Kappers M J, Jain M, Kovács A, Wallis D J and Oliver R A 2020 Alloy segregation at stacking faults in zincblende GaN heterostructures *J. Appl. Phys.* **128** 145703
[17] Church S A, Ding B, Mitchell P W, Kappers M J, Frentrup M, Kusch G, Fairclough S M, Wallis D J, Oliver R A and Binks D J 2020 Stacking fault-associated polarized surface-emitted photoluminescence from zincblende InGaN/GaN quantum wells *Appl. Phys. Lett.* **117** 032103
[18] Gundimeda A, Kusch G, Frentrup M, Kappers M J, Wallis D J and Oliver R A 2024 Cathodoluminescence studies of the optical properties of a zincblende InGaN/GaN single quantum well *Nanotechnology* **35** 395705
[19] Robin Y, Pristovsek M, Amano H, Oehler F, Oliver R A and Humphreys C J 2018 What is red? On the chromaticity of orange-red InGaN/GaN based LEDs *J. Appl. Phys.* **124** 183102
[20] Ding B, Frentrup M, Fairclough S M, Kusch G, Kappers M J, Wallis D J and Oliver R A 2021 Multimicroscopy of cross-section zincblende GaN LED heterostructure *J. Appl. Phys.* **130** 115705
[21] Xiu H, Fairclough S M, Gundimeda A, Kappers M J, Wallis D J, Oliver R A and Frentrup M 2023 Polarity determination of crystal defects in zincblende GaN by aberration-corrected electron microscopy *J. Appl. Phys.* **133** 105302
[22] Drouin D, Couture A R, Joly D, Tastet X, Aimez V and Gauvin R 2007 CASINO V2.42—a fast and easy-to-use modeling tool for scanning electron microscopy and microanalysis users *Scanning* **29** 92
[23] Miller, M K, Russell K F, Thompson K, Alvis R and Larson D J 2007 Review of atom probe FIB-based specimen preparation methods *Microsc. Microanal.* **13** 428–36
[24] Thompson K, Gorman B, Larson D, van Leer B and Hong L 2006 Minimization of Ga induced FIB damage using low energy clean-up *Microsc. Microanal.* **12** 1736–7
[25] Someya T, Akiyama H and Sakaki H 1996 Enhanced binding energy of one-dimensional excitons in quantum wires *Phys. Rev. Lett.* **76** 2965
[26] Lee L Y, Frentrup M, Vacek P, Kappers M J, Wallis D J and Oliver R A 2019 Investigation of stacking faults in MOVPE-grown zincblende GaN by XRD and TEM *J. Appl. Phys.* **125** 105303